Supplementary material in addition to SR-Site modeling report TR-10-11 as requested by SSM

2.0 The distribution of saturation times in the Forsmark repository

1.5 The effect of hydraulic connections between deposition holes

Daniel Malmberg, Mattias Åkesson, Ola Kristensson

Clay Technology AB, Lund, Sweden

December 2013

Table of Contents

1 **Task 2:** Distribution of saturation times

As part of the evaluation of SKB's license application, SSM has requested that the distribution of the buffer's saturation time in all the deposition holes is analysed. Here we use data from groundwater models of the Forsmark repository, and couple this with thermo-hydraulic models of the buffer saturation process in deposition holes and hydraulic models of the saturation process in the tunnel backfill to estimate the distribution of saturation times.

1.1 Background – Summary of results from SR-site

In task 3 of the SR-site THM modelling report (Åkesson et al. 2010) several models were constructed to estimate the maximum and minimum saturation time for three different types of deposition holes. These were:

- Deposition holes intersected by a single fracture at the mid-height of the canister (CMH-fracture)
- Deposition holes with no fractures, but where the tunnel just above the deposition hole is intersected by a single fracture (T-fracture)
- Deposition holes with no nearby fractures, and no nearby tunnel fractures (unfractured rock)

The models simulated thermo-hydraulic (TH), but not mechanical processes in the buffer, thus neglecting the consequences of the swelling of the bentonite buffer. To estimate the uncertainty introduced with this simplification, two models were constructed for each case: one with the buffer in the installation state and one with the buffer in a radially homogenized (extreme final) state. The assumption, supported by the findings in Task 3 of Åkesson et al. (2010) is that the actual time to reach full saturation is bounded by the saturation times found in these two models.

Furthermore, in Task 2 of Åkesson et al. (2010) the saturation time of the tunnel backfill was investigated using hydraulic models. Of primary interest for the present study is the models used to analyse the saturation time when water is only transported to the tunnel via fractures.

In Åkesson et al. (2010) no attempt to couple the results of Task 2 and 3 with the expected distribution of fractures intersecting deposition holes and deposition-hole tunnels in the Forsmark repository were done. Thus, the distribution of saturation times for all deposition holes was not evaluated. Here such an evaluation is presented; the data on the expected inflow characteristics are taken from groundwater models of the Forsmark repository prior to installation (Joyce et al. 2013). These are similar to the models of the excavation phase presented as part of SR-Site (Svensson & Follin 2010), but in difference to those, where a continuum model was used to describe the flow properties of the rock, Joyce et al. (2013) have implemented a discrete fracture network. This means that individual fractures are represented, and thereby also the fracture intersections with deposition holes and tunnels. The statistical fracture model used is taken from the modelling of the operational phase during periods with temperate climate conditions presented in Joyce et al. (2010).

1.2 Groundwater models fracture statistics

We use groundwater models of the Forsmark repository where the period after excavation but before installation of the canister with spent fuel and the clay buffer (i.e. the inflows are measured during atmospheric conditions in the tunnels/deposition holes) was simulated, and analyse the fracture statistics (such as the fraction of deposition holes intersected by fractures, the fracture inflows and the distance from each deposition hole to nearby tunnel-intersecting fractures).

3

These open-repository fracture flows are then used to calibrate Code_Bright models, where at first atmospheric conditions are prescribed in both the deposition hole and the tunnel. Thereafter, the tunnel backfill/deposition-hole buffer is introduced and the saturation time calculated.

When studying the properties of the fracture population in the groundwater models, three main differences with the models in Åkesson et al. (2010) can be identified:

1) no matrix flow is included in the groundwater models,

2) most fractures intersecting deposition holes and tunnels have considerably lower inflows than what was used in Åkesson et al. (2010),

3) most deposition holes are not intersected by fractures and are situated quite far away from the nearest tunnel fracture. Thus, to estimate the saturation-time distribution, the tunnel-fracture separations analysed (6m and 24m) in Åkesson et al. (2010) appears to have been too small.

These three points are discussed in further detail below.

1. Matrix flow
The perhaps most influential uncertainty in this work is the rock-matrix flow. Measurements on intact (unfractured) borehole cores from Forsmark (Vilks 2007) suggest that intact rock samples on the decimetre-size scale have hydraulic conductivities between $K_M = 5 \cdot 10^{-12} - 4 \cdot 10^{-14}$ m/s. However, in the groundwater models, all water is assumed to be transported in fractures. While the matrix flow may be unimportant when studying the transport of radionuclides out of the repository (as is the main goal of the groundwater models), it can, depending on its magnitude, almost completely set the distribution of saturation times, t_s, in the repository.

As the value of the matrix conductivity in Forsmark is uncertain, the distribution of saturation times has here been calculated assuming no matrix flow (i.e. water to the deposition holes and tunnels only enters through fractures). Then, Code_Bright models with different values of the matrix conductivity ($K_M = 10^{-11} - 10^{-14}$ m/s) have been used to calculate the saturation time $t_S(K_M)$ if water only enters via the matrix. The cumulative distribution of saturation times for a particular value of K_M is then assumed to be identical to that with no matrix flow for $t < t_S(K_M)$ and equal to 1 for $t > t_S(K_M)$.

2. Fracture inflows in the groundwater models
The cumulative distribution of inflows in deposition-hole-intersecting fractures, q_{DH}, is shown in the left panel of Figure 1. About 60% of all these fractures have $q_{DH} < 10^{-4}$ L/min. In Åkesson et al. (2010), the saturation time was calculated for $q_{DH} = 0.1$ L/min and 10^{-3} L/min, respectively.

The cumulative distribution of inflows through tunnel-intersecting fractures (q_{TF}) is shown in the right panel of Figure 1. As can be seen, the tunnel-fracture inflows vary between approximately $q_{TF} = 10^{-6}$ and $q_{TF} = 10$ L/min. It is important to note that in the groundwater models used here, grouting is not included and tunnel-intersecting fractures with inflows higher than the prescribed limit of 0.1 L/min (SKB 2010a) are included. If grouting were included this could change the inflows into the tunnels by reducing the inflow through high-flowing fractures and possibly (by redistribution of flow) increasing the inflow through low-flowing fractures. Hence, depending on how high-flowing fractures are handled in the Forsmark repository, the tunnel-backfill-saturation process could, in some tunnels, be rather different than the estimates presented in this report.

4

The models of the tunnel backfill saturation process presented in Åkesson et al. (2010) were set up using fractures with open-repository inflows equal to 0.1 L/min and 10^{-3} L/min only, hence to better represent the inflows expected in the repository we have here also included tunnel-intersecting fractures with $q_{TF} = 10^{-5}$ L/min.
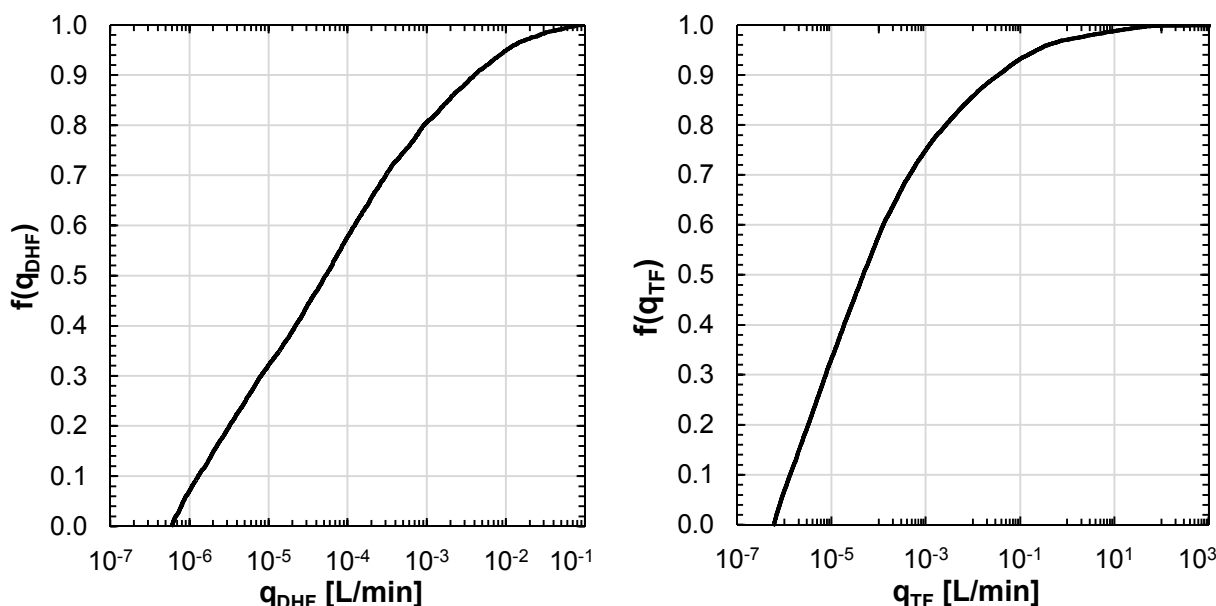

Figure 1. *Cumulative distribution of inflows (during atmospheric conditions in the repository) through deposition-hole intersecting fractures (left panel), and through tunnel-intersecting fractures (right panel), as determined in the groundwater models of the Forsmark repository.*

3. Fracture separation

The majority (about 90%) of deposition holes in the groundwater models are not intersected by fractures[1]. Furthermore, the vast majority of these deposition holes are situated far away from the nearest tunnel fracture.

To quantify the tunnel-fracture separation, L (see *Figure 2*), we can construct the cumulative distribution. In this report we will use the quantity *L/2*, i.e. the fracture separation divided by 2, as this is the quantity which is varied in the Code_Bright models presented in Åkesson et al. (2010) and below.

---

[1]This statement is only correct if EDZ (Excavation Damaged Zone) fractures are not included. In SR-site it is assumed that no significant EDZ will be present in Forsmark, and the same is assumed here. In section 1.5 a short discussion on the possible effects of a highly unrealistic EDZ is included.
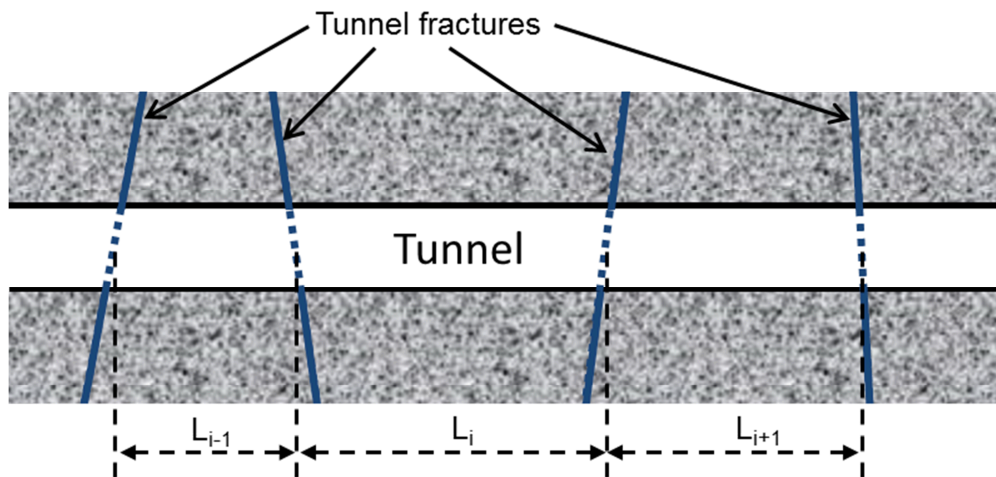
Figure 2. The tunnel-fracture separation, L, is defined as the separation between two fractures, as measured from the point were they intersect the deposition-tunnel central axis.

The cumulative distribution of *L/2* can be constructed in two different ways: 1) by analysing the fracture separations from the point of view of an observer sequentially positioned in each and every tunnel, or 2) from the point of view of an observer sequentially positioned in each and one of the deposition holes. In the first case, each fracture separation is only counted once and it results in the distribution identified by the black solid line in Figure 3. In the second case, each large fracture separation will be counted many times, as more deposition holes are situated between fractures with large separations than between fractures with small separations. The resulting distribution is the red solid line in Figure 3, which reaches a value of one at $L/2 \approx 260$m. When analysing the saturation-time distribution, the interesting statistic is the second one.

It should be noted that we have only considered the value of *L/2* for the two fractures situated closest to the deposition hole; if these have very low inflows, fractures further away have to be considered when analysing the tunnel-backfill-saturation time at a given position. In principle this could lead to that larger separations than *L/2= 260*m should be considered; however, with the data analysed here this was not the case.

As is seen, the majority (about 80%) of deposition holes are situated between fractures with *10* m $\leq L/2 \leq 100$ m, whereas in Åkesson et al. (2010) only *L/2 = 3* and *12* m were considered.
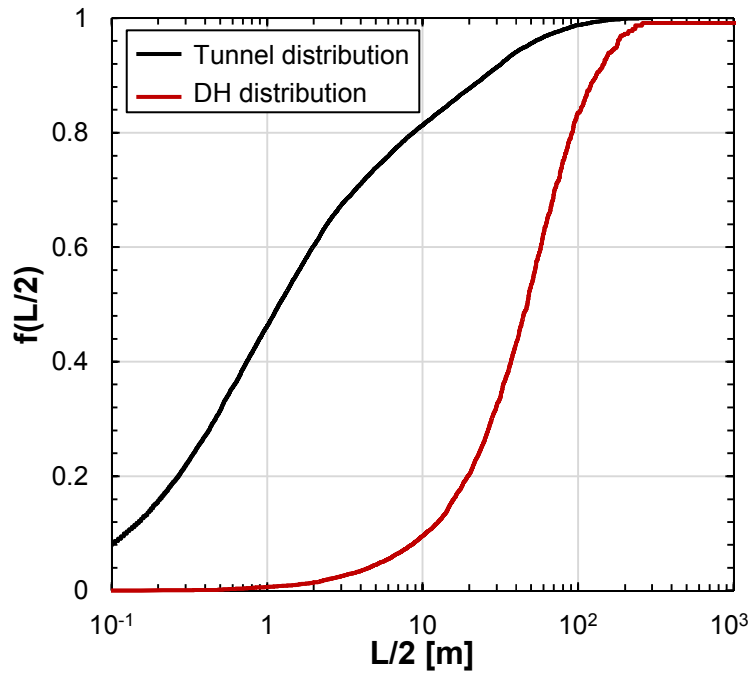
6

Figure 3. *Distribution of tunnel-fracture separations, where the tunnel-fracture separation, L, has been divided by a factor of 2. The black line shows the distribution from the point of view of an observer standing in the tunnels and the red line shows the distribution from the point of view of an observer standing in the deposition holes.*

When considering the saturation time of the tunnel backfill, at any given deposition point, it is to a first approximation set by 1) the separation between the two nearest surrounding fractures ($L/2$), 2) the inflow through these fractures (q_{TF}), and 3) the distance to the nearest fracture (d_{min}). In practice this method gives too slow saturation times, as more distant but higher flowing fractures can lead to a shorter saturation time, which partially can be handled by analysing all fractures/fracture pairs in the tunnel (this is further explained in section 1.5).

The distance to the nearest fracture (d_{min}) is of little significance when $L/2$ is small, but dominant when $L/2$ is large. This can be illustrated using the models of the tunnel backfill saturation phase which were presented in Task 2 in Åkesson et al. (2010). As part of that task, the saturation of the tunnel backfill was studied in the case where water only entered through equidistant fractures. Two fracture separations were investigated ($L/2= 3$ and 12 meters) using the geometry seen in Figure 11. The saturation profile at several different points in time after installation is shown in Figure 4 (left panel: $L/2=3$m, right panel: $L/2=12$m). As can be seen, the saturation profile in the two cases is rather different. When the fractures are relatively close to each other ($L/2=3$m, left panel) the saturation profile is rather shallow, and the entire buffer segment between the two fractures reach full saturation at approximately the same time. However, for larger fracture separations, a clear "saturation front" is seen in the tunnel backfill, with the parts close to the fracture reaching full saturation much faster than the parts further away.
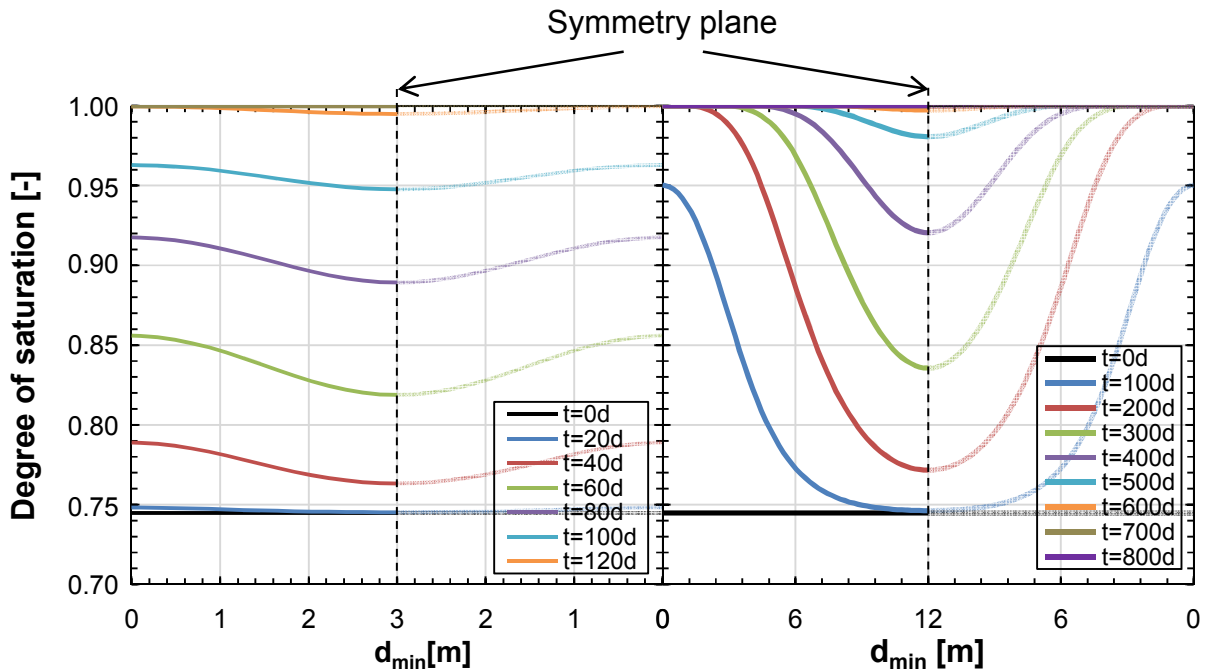
Figure 4. *Saturation profiles at the center of the tunnel backfill at different points in time after installation. The models are constructed with a symmetry plane in between the two fractures (see Figure 11), which, in these two models, were calibrated such as to give 10^{-3} L/min each under atmospheric conditions in the tunnel. The left panel depicts the evolution when the two fractures are separated by a distance of 6m, while the right panel depicts the evolution when the fractures are separated by 24m.*

1.3 Estimate of saturation time for different deposition holes

The saturation time of each deposition hole will here be calculated assuming none (or very small) matrix flow. The effect of the matrix flow is then taken into account when constructing the total distribution of saturation times.

We start by dividing the deposition holes into four different classes:

1) deposition holes which are intersected by one or more fractures, which set the saturation time,

2) deposition holes with no fractures, which are situated in between two tunnel fractures with small separation,

3) deposition holes with no fractures, which are situated in between two tunnel fractures with large separation, and

4) deposition holes with no fractures, which are situated in a tunnel with no fractures

Considering the deposition holes in class 1, the modelling done in Åkesson et al. (2010), where the saturation time was calculated due to water inflow through a fracture intersecting the deposition hole at mid height of the canister, gives a good estimate of the saturation time if the fracture inflow under atmospheric conditions is around 10^{-4} L/min or higher and a significant matrix flow is present. However, as can be seen in the left panel of Figure 1, the majority of deposition-hole-intersecting fractures have much lower inflows. Thus, to properly cover the range of inflow configurations found in the groundwater models, we must update the models from Åkesson et al. (2010) by including a very low matrix flow, and add a model with a low-flowing fracture.

It should be pointed out that some of the deposition holes that belong to class 1 will have such a low fracture inflow that the saturation time is actually set by nearby tunnel fractures (i.e. the deposition hole is saturated by water entering via the tunnel backfill). Here this is handled by comparing the saturation time as calculated from deposition-hole-intersecting fractures and tunnel-intersecting fractures separately, with the assumption that the shortest one is valid. In reality the two inflows will add up, potentially leading to significantly shorter saturation times. The number of deposition holes which this is the case for is, however, low, and thus have small impact on the shape of the cumulative distribution curve of saturation-times.

Concerning deposition holes belonging to class 2 and 3, we can estimate the saturation time by calculating the time it will take until the tunnel backfill is saturated above the deposition hole. Models for two fracture separations were analysed in Task 2 of Åkesson et al. (2010); these are here supplemented by 18 additional models, which better cover the range of fracture inflows and fracture separations present in the groundwater models.

Deposition holes belonging to class 4 will be saturated either through matrix flow or, alternatively, by water passing through the tunnel plug into the deposition tunnel from the transport tunnels. In the latter case, we have no way of estimating the time until saturation in this report, and thus when zero matrix flow is assumed, the saturation time of the class 4 deposition-holes will be set to infinity. This is, however, of little importance for the saturation-time distribution, as the fraction of deposition holes belonging to class 4 is less than one per cent.

1.4 Additional models

As mentioned above, several new models were constructed (with respect to those presented in Åkesson et al. 2010) to better represent the inflow characteristics in the groundwater models. Below we first discuss the additional models of the deposition-hole saturation process, where after we describe the additional models of the tunnel-backfill saturation process.

1.4.1 Additional models of the deposition-hole saturation process

The hydration of the buffer in a deposition hole intersected by a single fracture was analysed in Task 3 of Åkesson et al. (2010). Two fracture transmissivities were used, corresponding to fracture inflows under atmospheric conditions of $q_F = 0.1$ L/min and $q_F = 10^{-3}$ L/min. The simulations also included matrix flow, with $K_m = 10^{-11}$ m/s and $K_m = 10^{-12}$ m/s, respectively. Two combinations of these fracture transmissivities and matrix conductivities were modelled: $q_F = 0.1$ L/min with $K_m = 10^{-11}$ m/s and $q_F = 10^{-3}$ L/min with $K_m = 10^{-12}$ m/s. For the purposes here, however, we would like to know the time until full saturation in the buffer for $q_F = 0.1$ L/min, 10^{-3} L/min and 10^{-5} L/min in the case of a very small matrix flow.

The models presented use the same geometry and mesh, as well as material parameters and initial/boundary conditions, as was used in Åkesson et al. (2010). For completeness they are briefly described below; for a more in-depth description, as well as motivation for the values used the reader is directed to Task 3 in Åkesson et al. (2010).

Material parameters
The constitutive laws used are:

Liquid and gas density

$$\rho_l = 1002.6 \cdot \exp[4.5 \cdot 10^{-4}(p_l - 0.1 \text{ MPa}) - 3.4 \cdot 10^{-4}T] \tag{1-1}$$

$$\rho_g = \frac{0.018p_v}{8.3143(273.15 + T)} \cdot RH \tag{1-2}$$

$$p_v = 130675 \cdot \exp\left[-\frac{5239.7}{273.15 + T}\right] \tag{1-3}$$

$$RH = \exp\left[\frac{-0.018 \cdot (p_g - p_l)}{8.3143 \cdot (273.15 + T) \cdot \rho_l}\right] \tag{1-4}$$

Conductive heat flux

$$\boldsymbol{i}_c = -\lambda \nabla T \tag{1-5}$$

$$\lambda = \lambda_{sat} \cdot S_l + \lambda_{dry} \cdot (1 - S_l) \tag{1-6}$$

Retention behaviour, Van Genuchten

$$S_l = \left[1 + \left(\frac{S_l}{P_0}\right)^{1/(1-\lambda)}\right]^{-\lambda} \tag{1-7}$$

$$S_l = p_g - p_l$$

Flow through porous medium

$$\boldsymbol{q}_l = -\frac{k \cdot k_{rl}}{\mu_l} \nabla \boldsymbol{p}_l \tag{1-8}$$

Buffer materials: $k_{rl} = S_l^3$ (1-9)

Rock materials: $k_{rl} = \sqrt{S_l}\left[1 - \left(1 - S_l^{1/\lambda}\right)^\lambda\right]^2$ (1-10)

$$\mu_l = 2 \cdot 10^{-12} \exp\left(\frac{1808.5}{273.15 + T}\right) \tag{1-11}$$

Vapour diffusion

$$\boldsymbol{i}_g^w = -\left[n\rho_g(1 - S_l)D_m^w\right]\nabla\omega_g^w \tag{1-12}$$

$$D_m^w = \tau \cdot 5.9 \cdot 10^{-6} \frac{(273.15 + T)^{2.3}}{p_g} \tag{1-13}$$

The models simulate thermo-hydraulic, but not mechanical processes in the buffer. This introduces an uncertainty in the saturation time, as the swelling of the buffer and its effect on the void ratio distribution and hydraulic properties of the clay are not included. To estimate the effect of this simplification two "mechanical" states of the buffer were modelled; 1) the initial state and 2) the homogenised state. In 1) the buffer is modelled in the state it had just after installation, while in 2) it is modelled in a theoretical final state, where the buffer has swelled (radially) and homogenised in that direction. The parameters used to describe the buffer in the initial state models are summarised in Table 1-1, while the parameters in the homogenised models are found in Table 1-2.

Table 1-1. Data used for initial state MX-80 materials. Directly adopted from the values used in Åkesson et al. (2010).

Parameter		Buffer ring n=0.36 w=17%	Buffer cylinder n=0.61 w=17%	Buffer pellets n=0.61 w=17%	Backfill block n=0.39 w=17%	Backfill Pellets n=0.61 w=17%
Thermal conductivity	λ_{dry} λ_{sat} (W/mK)	0.7 1.3	0.7 1.3	0 1.3	0.7 1.3	0 1.3
Specific heat	c (J/kgK)			800		
Solid density	ρ_s (kg/m^3)			2780		
Intrinsic permeability	k (m^2)	$1.2\cdot10^{-21}$	$2.0\cdot10^{-21}$	$5.2\cdot10^{-19}$	$2.1\cdot10^{-21}$	$5.2\cdot10^{-19}$
Relative permeability	k_{rl} (-)			S_r^3		
Vapour diffusion tortuosity	τ (-)			1		
Water retention curve	P_0 (MPa) λ (-)	67.2 0.48	43.5 0.38	0.508 0.26	37.2 0.34	0.162 0.19

Table 1-2. Data used for homogenized MX-80 materials. Directly adopted from the values used in Åkesson et al. (2010).

Parameter		Homog. Buffer cylinder n=0.419 w=17%	Homog. Buffer ring n=0.435 w=17%	Homog. Backfill n=0.454 w=17%
Thermal conductivity	λ_{dry} λ_{sat} (W/mK)		0.7 1.3	
Specific heat, Solid density	C (J/kgK) ρ_s (kg/m^3)		800 2780	
Intrinsic permeability	k (m^2)	$4.2\cdot10^{-21}$	$6.0\cdot10^{-21}$	$8.9\cdot10^{-21}$
Relative permeability	k_{rl} (-)		S_r^3	
Vapour diffusion tortuosity	τ (-)		1	
Water retention curve,	P_0 (MPa) λ (-)	15.19 0.25	8.93 0.22	5.85 0.21

To determine the properties of the Homogenized Backfill the tunnel geometry was obtained as an average of the measures of the "Theoretical section" and the "Maximum fall out" as defined in the Backfill Production Report (SKB 2010a). The "Averaged" geometry was then used to find suitable properties of the homogenized tunnel backfill materials: backfill blocks and pellets.

The parameters used to model the rock and canister materials are found in Table 1-3. The value of the rock intrinsic permeability deserves some discussion. The goal of this modelling is to quantify the saturation time due to fracture wetting without significant matrix flow. Thus, in principle the intrinsic permeability of the rock should be set as low as possible. However, setting too small a value leads to unrealistically high liquid pressures in the rock around the deposition hole, due to the increased temperature that causes the water to expand (see equation 1-1) in combination with the low permeability, which prevents the water to flow away from the warm zone. Using the value 10^{-21} m/s is a good compromise which leads to a very low matrix flow, while avoiding high pressures in the rock.

Table 1-3. Data used for the rock, fracture and canister materials. Directly adopted from the values used in Åkesson et al. (2010).

Parameter		Rock n=0.003	Fracture n=0.99	Canister n=0.0001
Thermal conductivity	$\lambda_{dry} = \lambda_{sat}$ (W/mK)	2.8	2.8	90
Specific heat	C (J/kgK)	770	770	480
Solid density	ρ_s (kg/m^3)	2277	2277	7500
Intrinsic permeability	k (m^2)	10^{-21}	$4.3\cdot10^{-15}$ $4.3\cdot10^{-17}$ $4.3\cdot10^{-19}$	-
Relative permeability	k_{rl} (-)	$\lambda= 0.6^{(*)}$	S_r^3	-
Vapour diffusion tortuosity	τ (-)	1	1	-
Water retention curve	P_0 (MPa) λ (-)	1.74 0.6	1.74 0.6	-

$^{(*)}$ van Genuchten is used, see equation 1-7.

Geometry, initial and boundary conditions

The geometry is a two-dimensional axisymmetric representation of a single deposition hole, with the backfilled tunnel and nearby host rock; it is shown in Figure 5.

The initial conditions prescribed are taken from Åkesson et al. (2010). They are:

Parameter	Initial liquid pressure	Porosity	Initial temperature
Unit	[MPa]	[-]	[°C]
Rock/Fracture	4 - 5.2[1]	0.003	15
Buffer rings	-46	0.36	15
Buffer blocks	-46	0.38	15
Buffer pellets	-46	0.64	15
Backfill blocks	-46	0.39	15
Backfill pellets	-46	0.64	15
Canister	-46	0.0001[2]	15

[1] Linear vertical distribution between upper (4MPa) and lower (5.2MPa) boundary

[2] When using Code_Bright all materials must have a porosity. As the canister in reality has zero porosity a very low value is prescribed here.
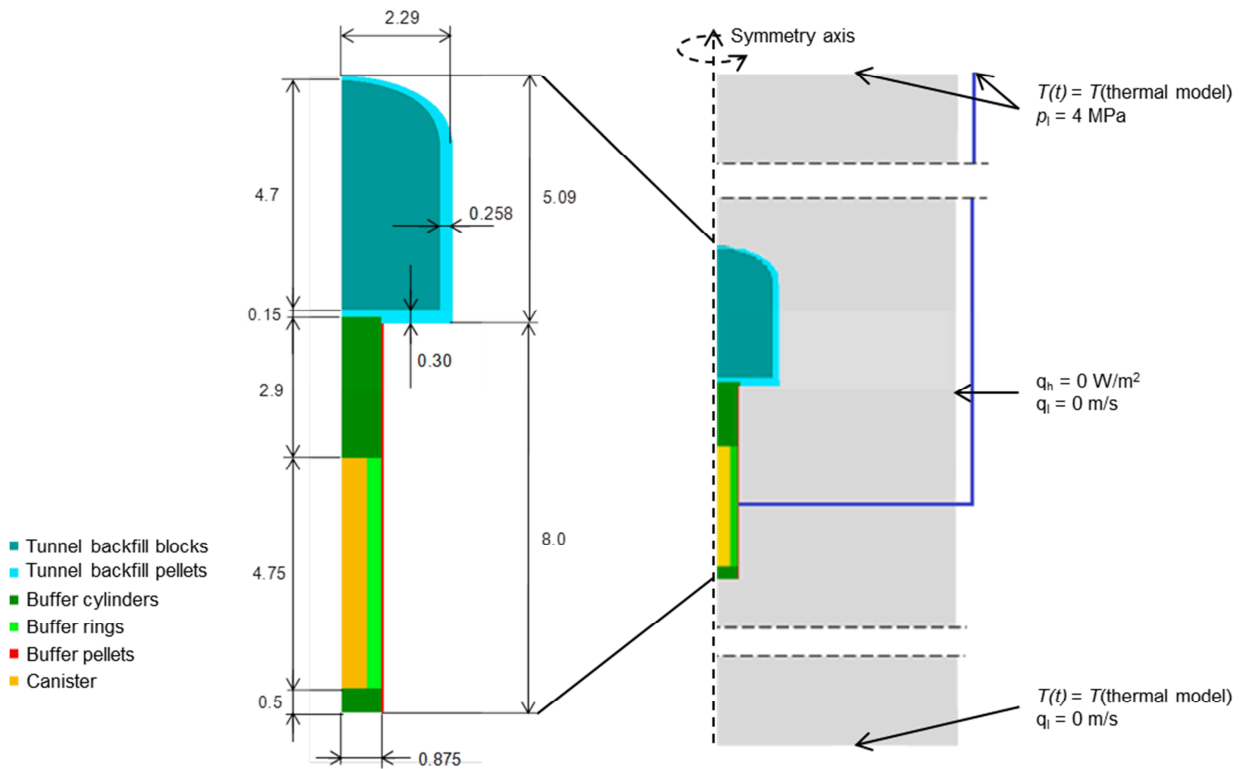
Figure 5. *Geometry and boundary conditions used to model the saturation process in a deposition hole intersected by a single fracture at canister mid height. The figure is adapted from figures 3-3 and 3-6 in Åkesson et al. (2010).*

Two types of thermal boundary conditions are used, a heat flux on the canister and a prescribed temperature on the upper and lower boundaries (on the vertical boundary adiabatic thermal conditions are prescribed). In Åkesson et al. (2010), all models were saturated within 3 000 years. For some models analysed here this was not the case, hence the boundary conditions had to be evaluated for considerably longer time periods (*t = 30 000* years).

The canister heat load is prescribed on two vertically orientated concentric cylinders within the canister material. 1/3 of the total heat load is prescribed at the radial distance $r = 0.105$ m and 2/3 of the total heat load at $r = 0.315$ m. This is done to mimic the real case, where four fuel elements are placed in the inner part and eight in the outer part of the canister.

The heat load (i.e. the canister power) is prescribed according to the expression reported in Hökmark et al. (2010):

$$P(t) = P(0) \sum_{i=1}^{i=i_{\max}} a_i \exp(-t/t_i), \tag{1-14}$$

where *P(0) = 1700* W, $i_{\max} = 7$ and the parameters a_i and t_i have the values shown in Table 1-4. We here assume that it is valid for *t ≤ 30 000* years, the graph in Figure 6 shows the values during this time span.

Table 1-4. Decay function coefficients and the corresponding canister power graph.

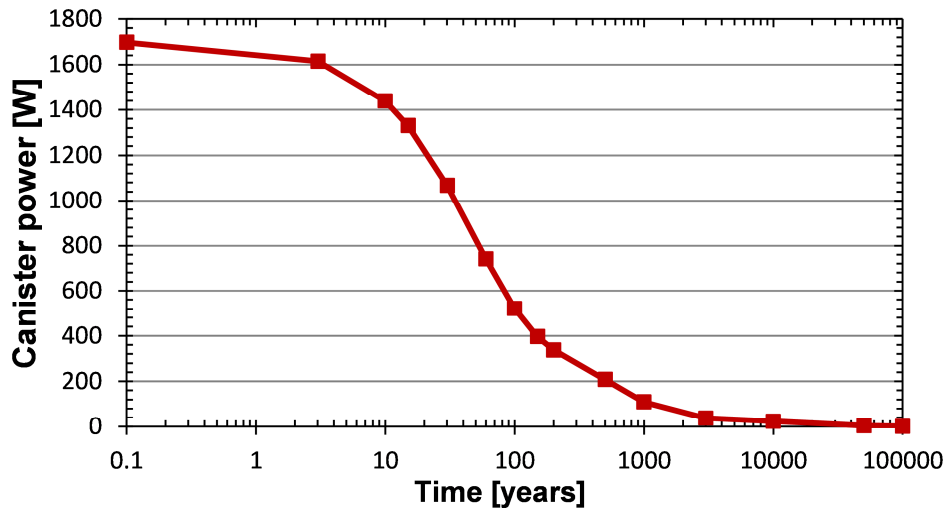| i	1	2	3	4	5	6	7
t_i	20	50	200	500	2000	5000	20000
a_i	0.060	0.705	-0.055	0.250	0.025	-0.009	0.024

Figure 6. *Canister power as calculated using equation 1-14.*

The temperature prescribed on the upper and lower boundaries are taken from a thermal model of the entire repository used in the THM report concerning the geosphere, as presented in Hökmark et al. (2010). That model simulated the entire repository with surrounding rock mass, assuming a canister distance of 6m - 6.8m (depending on the position within the repository) and a rock thermal conductivity equal to 3.57 W m^{-1} K^{-1}. The temperature change 60 m above/below the repository level is shown in Figure 7 (red and blue solid lines). As can be seen the evolution is almost identical, hence the same temperature could be prescribed on both boundaries (black dashed line in Figure 7). Data for t>10 000 years have not been directly evaluated at +/- 60 m above/below the deposition holes, but the temperature evolution on the deposition-hole wall in similar models is available in Hökmark et al. (2010). The results suggest that the temperature reaches its original value (T=15°C) about 100 000 years after installation of the spent fuel, and that the trend, as plotted on a semi-log plot, is close to linear between 10 000 and 100 000 years. As such the temperature boundary condition has been extrapolated as is shown in Figure 7. It should be noted that the temperature at the boundary is less than 4°C above its original value of 15°C in this time interval. As such, any small errors in the temperature boundary condition should have a very small effect on the thermo-hydraulic evolution in the buffer.
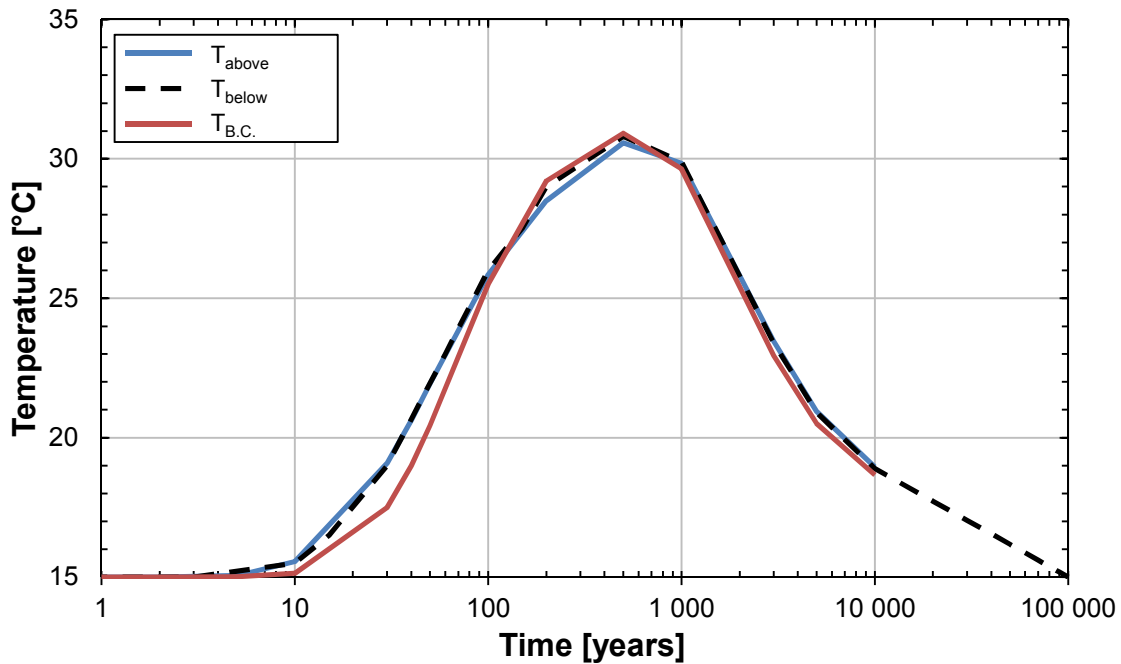
14

Figure 7. Temperature change at the upper (red line) and lower (blue line) boundary of the model, taken from a thermal simulation of the entire repository presented in Hökmark et al. (2010). The dashed black line is the temperature boundary condition prescribed on the boundary in the Code_Bright models.

The hydraulic boundary condition was evaluated from a hydraulic model of the entire repository, presented in Åkesson et al. (2010). It showed that at both the upper and lower boundaries of the model used to simulate the evolution of a single deposition hole, the liquid pressure was close to hydrostatic at all times. Furthermore, evaluation of the single-deposition-hole model showed that a no-flow condition on the lower boundary gave a correct evolution. As such, the only hydraulic boundary condition used in the model is that a liquid pressure of 4 MPa is prescribed on the upper boundary of the geometry.

1.4.1.1 Parameter variations explored

The main parameter to be investigated here is the fracture transmissivity, T_F. However, it is more correct to state that the importance of variations in fracture inflow was explored, as the values of these, as measured under atmospheric conditions, were used to calibrate the transmissivity. Aside from different fracture transmissivities, one extra (with respect to the models presented in Åkesson et al. 2010) value of the matrix hydraulic conductivity was modelled, $K_m = 10^{-14}$ m/s. The different models analysed are summarised in Table 1-5 below.

Table 1-5. Additional models constructed to explore the effect of deposition-hole intersecting fractures on the buffer's saturation time.

Model name	Matrix conductivity K_m [m/s]	qF [L/min]	I/H[1]
Km14_qF1_I	10^{-14}	0.1	I
Km14_qF1_H	10^{-14}	0.1	H
Km14_qF3_I	10^{-14}	10^{-3}	I
Km14_qF3_H	10^{-14}	10^{-3}	H
Km14_qF5_I	10^{-14}	10^{-5}	I
Km14_qF5_H	10^{-14}	10^{-5}	H
Km14 _I	10^{-14}	-	I
Km14 _H	10^{-14}	-	H

[1] I = **I**nstallation state, H = **H**omogenised state

1.4.1.2 Results

In accordance with Åkesson et al. (2010), the saturation time (here defined as the time from buffer installation until the buffer reaches 99% saturation) was measured in four pre-determined points (P1 – P4) as well as in the last point to reach full saturation. The positions of points P1-P4 are illustrated in Figure 8. It should be noted that due to limitations of the post-processor used, the saturation has to be measured on the second node from the edge of the buffer material (the same is true for the models presented in Åkesson et al. 2010).
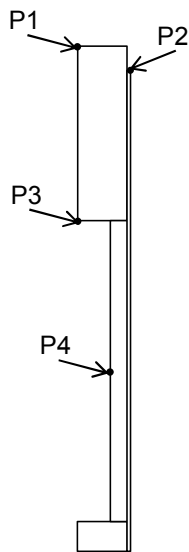

Figure 8. Schematic overview of the position of the four points in the buffer where the saturation time is recorded in each model.

In Figure 9 the time to reach full saturation in the six models with $K_m = 10^{-14}$ m/s and a single fracture is shown. The saturation times are rather long, with a time to saturation of *679 - 1 579* years for $q_F = 0.1$ L/min up to *2 035 - 2 551* years when $q_F = 10^{-5}$ L/min. Furthermore, it can be observed that the results of the models with $q_F = 0.1$ and 10^{-3} L/min are rather similar, hence in these cases the buffer limits the fracture flow.

Another important aspect here is when we define the deposition hole to be saturated. As is seen in Figure 9, points 3 and 4 are in general saturated much faster than points 1 and 2.

16

Hence, if we defined the saturation time as the time until saturation just around the canister the result would be rather different from if we define it as the time until the buffer in the entire deposition-hole is saturated. Following the procedure used in Åkesson et al. (2010) we will here use the latter definition, i.e. the saturation time is defined as the time it takes to saturate the buffer in the entire deposition hole.
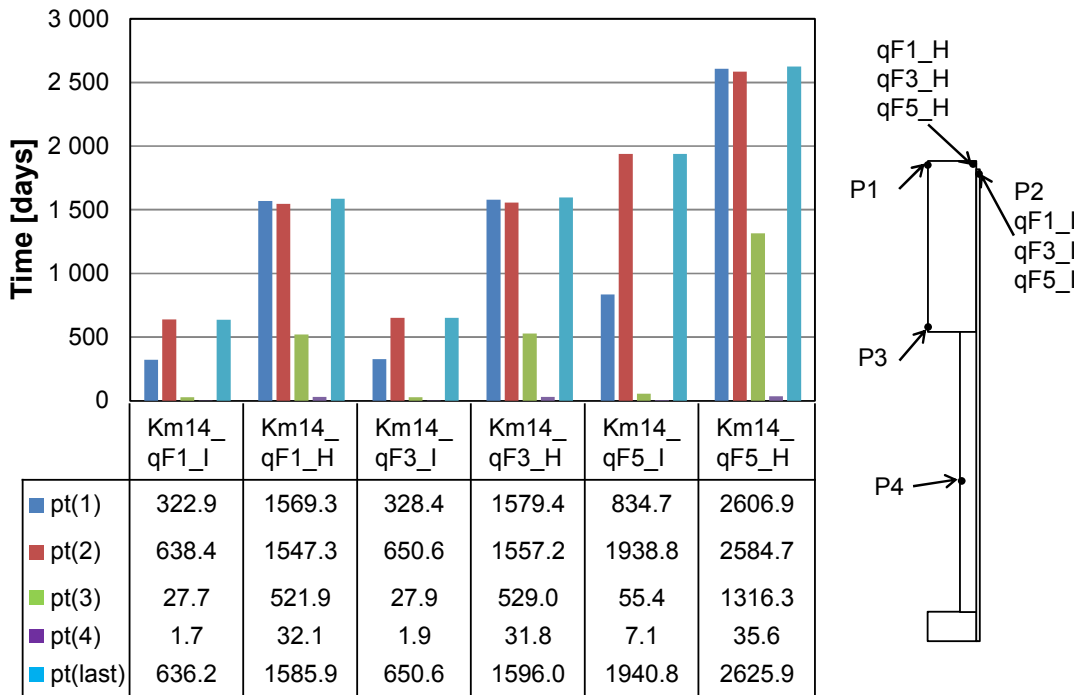

	Km14_qF1_I	Km14_qF1_H	Km14_qF3_I	Km14_qF3_H	Km14_qF5_I	Km14_qF5_H
pt(1)	322.9	1569.3	328.4	1579.4	834.7	2606.9
pt(2)	638.4	1547.3	650.6	1557.2	1938.8	2584.7
pt(3)	27.7	521.9	27.9	529.0	55.4	1316.3
pt(4)	1.7	32.1	1.9	31.8	7.1	35.6
pt(last)	636.2	1585.9	650.6	1596.0	1940.8	2625.9

Figure 9. *Time to 99% saturation [in years] in models with a matrix conductivity equal to 10^{-14} m/s and a fracture flow of $q_F = 0.1$ L/min (qF1_I, qF1_H), $q_F=10^{-3}$ L/min (qF3_I, qF3_H) and $q_F=10^{-5}$ L/min (qF5_I, qF5_H). A description of the parameter variations between the models is shown in Table 1-5.*

In Figure 10, the saturation time due to only matrix flow is shown for $K_M = 10^{-11}$, 10^{-12}, 10^{-13} and 10^{-14} m/s. Only the models with 10^{-14} m/s were done as part of this report, the results for the other six cases are taken from Åkesson et al. (2010). The models have been re-named to fit the nomenclature in this report, although their original names are also included in Figure 10. As can be seen the saturation time scales rather well with the matrix conductivity, a decrease of K_M with a factor of 10 leads to an increase in saturation time of roughly a factor of 10.

It is also important to compare the saturation time for $K_M = 10^{-14}$ m /s and no fracture (*17 742 – 21 872*) with the maximum saturation time seen when including fractures (*1 941 – 2626* for $q_F = 10^{-5}$ L/min). This indicates that the matrix plays a very small role in saturating the buffer in the fracture models.
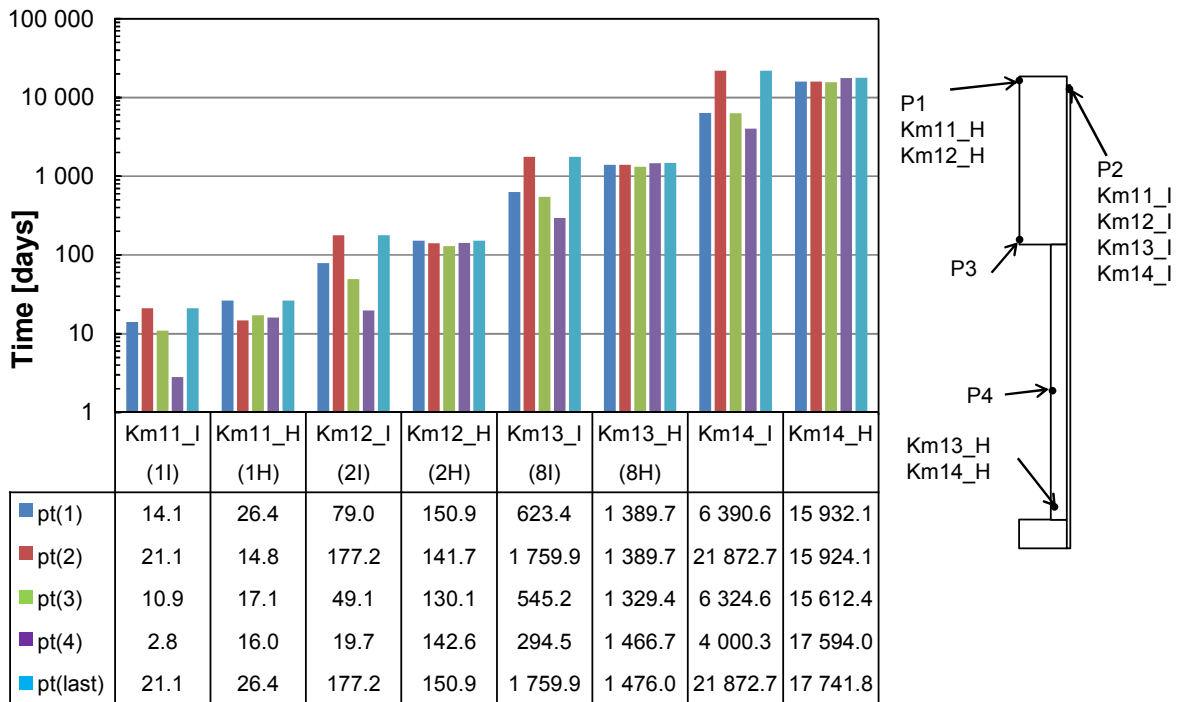
| | Km11_I | Km11_H | Km12_I | Km12_H | Km13_I | Km13_H | Km14_I | Km14_H |
	(1I)	(1H)	(2I)	(2H)	(8I)	(8H)		
pt(1)	14.1	26.4	79.0	150.9	623.4	1 389.7	6 390.6	15 932.1
pt(2)	21.1	14.8	177.2	141.7	1 759.9	1 389.7	21 872.7	15 924.1
pt(3)	10.9	17.1	49.1	130.1	545.2	1 329.4	6 324.6	15 612.4
pt(4)	2.8	16.0	19.7	142.6	294.5	1 466.7	4 000.3	17 594.0
pt(last)	21.1	26.4	177.2	150.9	1 759.9	1 476.0	21 872.7	17 741.8

Figure 10. *Time to reach 99% saturation [in years] in the deposition-hole buffer in models with only matrix flow (i.e without a fracture). The models with matrix conductivity equal to 10^{-13} m/s and above were done as part of Åkesson et al. (2010) and the results are taken directly from that report. The model identifiers used in that report are included inside parenthesis in the figure.*

1.4.2 Additional models of the tunnel-backfill saturation process

Setup

The models presented here to analyse the tunnel-backfill saturation process used the same type of geometry and the same material parameters (with the exception of one additional value of the fracture transmissivity) as the models in Åkesson et al. (2010). An example of the geometry is shown in Figure 11, where the model with *L/2 = 3* is shown.
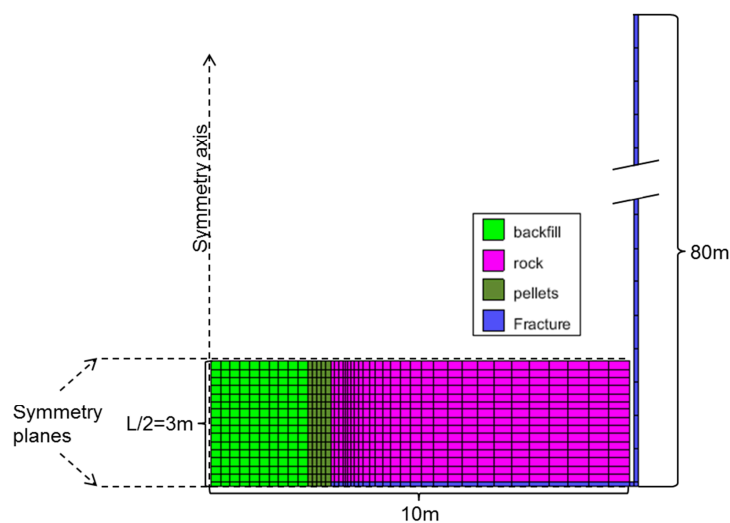

Figure 11. *Geometry used when modelling fracture wetting of the tunnel backfill. In this particular model the inter-fracture distance (L) was 6m. To achieve a relevant liquid pressure at the intersection of the no-flow boundary (r=10m) the fracture length is set to 80m. A more*

18

in-depth description of the geometry shown here and how it was constructed can be found in section 2.3 of Åkesson et al. (2010).

Several different models were constructed, varying the fracture half separation, *L/2*. The values of *L/2* were chosen so as to represent the cumulative distribution of *L/2* (*f(L/2)*, see red solid line in Figure 3). The values of *L/2* modelled, and the corresponding value of *f(L/2)* are listed in Table 1-6. As can be seen the distribution is better mapped for *f(L/2) > 0.80*; this is motivated by the large variations in saturation time in this region.

Table 1-6. Range of L/2 modelled and the correponding values of the cumulative distribution function of L/2.

L/2 [m]	f(L/2)
3	0.03
20	0.20
38	0.40
60	0.60
90	0.80
130	0.90
170	0.95
260	0.99

The only difference in geometries between the models is that the backfill, pellets and rock materials were extended away from the fracture to the corresponding fracture half separation. The material parameters are summarized in Table 1-7. The constitutive laws used are the same as the hydraulic constitutive laws summarised in equation 1-1 to 1-11.

Table 1-7. Material parameters used when modeling the tunnel-backfill saturation process. Directly adopted from the values used in Åkesson et al. (2010).

Parameter		Backfill block $e=0.635$ $w=17\%$	Backfill Pellets $e=1.780$ $w=17\%$	Homog. Backfill $e=0.74$ $w=17\%$	Homog. Backfill $e=0.91$ $w=17\%$	Rock matrix	Fracture material
Porosity	n (-)	0.388	0.64	0.425	0.476	0.003	0.003
Intrinsic permeability	k (m^2)	2.1×10^{-21}	5.2×10^{-19}	4.8×10^{-21}	1.5×10^{-20}	5×10^{-20}	[1]
Relative permeability	k$_r$ (-)	S_r^3	S_r^3	S_r^3	S_r^3	vG[†]: $\lambda = 0.6$	vG[2)]: $\lambda = 0.6$
Water retention curve	P$_0$ (MPa) λ (-)	37.2 0.34	0.162 0.19	11.6 0.23	3.45 0.20	1.74 0.6	1.74 0.6

[1]Three variations: 2.5×10^{-15} m^2 (0.1 L/min) , 2.5×10^{-17} m^2 (10^{-3} L/min) and 2.5×10^{-19} m^2 (10^{-5} L/min)
[2)]vG: van Genuchten relative permeability law, see equation 1-10.

The models of the tunnel backfill saturation process done for this report are summarized in Table 1-8. There, q_{TF} is the tunnel fracture inflow in L/min as measured during atmospheric conditions.

Table 1-8. Overiew of models of the tunnel backfill saturation process.

q_{TF} / L/2	10^{-5}	10^{-3}	10^{-1}
3	TB_Q5_L3	TB_Q3_L3	TB_Q1_L3
20	TB_Q5_L20	TB_Q3_L20	TB_Q1_L20
38	TB_Q5_L38	TB_Q3_L38	TB_Q1_L38
60	-	TB_Q3_L60	TB_Q1_L60
90	-	TB_Q3_L90	TB_Q1_L90
130	-	TB_Q3_L130	TB_Q1_L130
170	-	TB_Q3_L170	TB_Q1_L170
260	-	TB_Q3_L260	-

Results

The results from the models were quantified by measuring the time until $S_l = 0.99$ at distance d_{min} from the fracture at $r = 2.55$ m (i.e. in the pellets column). Here $d_{min} = n \cdot 6$ m, where n goes from *1* up to n_{max}, such that $(L/2 – 6) \le n_{max} \cdot 6$ m $< L/2$. In the cases where $n_{max} \cdot d_{min} \ne L/2$, the time until $S_l = 0.99$ at $L/2$ m from the fracture in the pellets column ($r = 2.55$ m) was also measured and recorded.

In Figure 12, the results from models with $q_{TF} = 10^{-3}$ L/min (solid lines) and $q_{TF} = 0.1$ L/min (dashed lines) are shown. As can be seen, the results for the two fracture inflows are rather similar. The cause is that for such high inflows, the bentonite limits the inflow, as it effectively acts as a seal on the fracture.
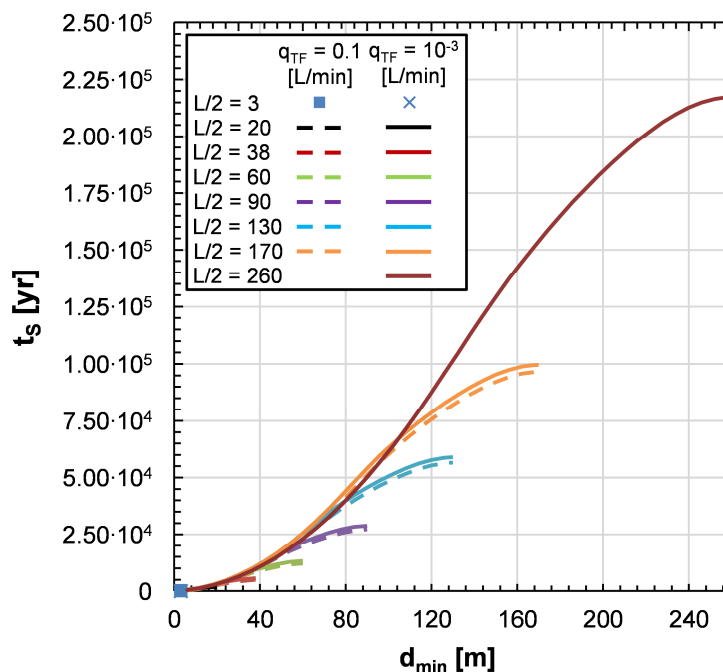

Figure 12. *The graph shows the saturation time as a function of distance to the nearest fracture, for seven different fracture separations. Solid lines correspond to a fracture inflow (under atmospheric conditions) $q_{TF} = 0.1$ L/min, and dashed lines to $q_{TF}=10^{-3}$ L/min.*

Not included in Figure 12 are the results from the three models with $q_{TF} = 10^{-5}$ L/min (see Table 1-8). For such a low inflow one might assume that the saturation time is entirely controlled by the flow in the fracture, i.e. the bentonite can, at all times during the hydration process, take in all the water which the fracture provides per unit time. Hence, the buffer does

not limit the inflow from the fracture. Under such conditions, the saturation time can to a good approximation be calculated analytically, by dividing the total available pore volume in the buffer with the steady-state fracture flow:

$$t_S = \frac{V_p}{q_{TF}}.$$ (1-15)

Here, V_p is the total available pore volume. We are, however, interested in the saturation time as a function of L/2, and hence we re-write equation 1-15 on the form:

$$t_S = \frac{A_T \times 2 \times L/2}{q_{TF}},$$ (1-16)

where, A_T is the available pore area of the deposition tunnel. Taking the value $A_T = 5.9$ m^2 (which is valid for the case of maximum fallout (see e.g. Åkesson et al. 2010) we find:

$$t_S = 2.245 \times 10^{-2} \times \frac{L/2}{q_{TF}} \text{ years,}$$ (1-17)

where q_{TF} is measured in units of L/min. If we assume that q_{TF}, as measured during atmospheric conditions, is unchanged by the tunnel backfill, we can thus calculate t_S given q_{TF} using equation 1-17.

The results from the three models with $q_{TF} = 10^{-5}$ L/min are shown in Figure 13. Also shown is the saturation time for each value of $L/2$ as calculated using equation 1-17. As is seen, the agreement is very good between the analytical solution and the numerical models. This reinforces the assumption made when deriving equation 1-17, that the fracture flow, for such low inflows, is not significantly changed by the presence of the tunnel backfill.

Furthermore, the numerical simulations with $q_{TF} = 10^{-5}$ L/min show that the tunnel backfill reaches full saturation on a rather similar time-scale at all distances from the fracture (see Figure 13), hence t_S is independent of the distance d_{min} between the fracture and the deposition hole, and hence to a good approximation only depends on the fracture half separation, $L/2$.
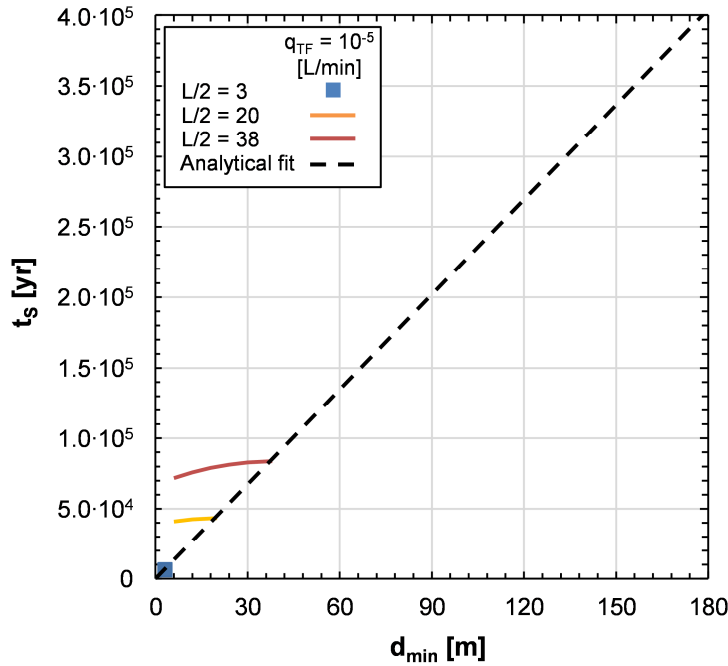
Figure 13. *The graph shows the saturation time as a function of distance to the nearest fracture, for three different fracture separations. Solid lines correspond to a fracture inflow (under atmospheric conditions) of q_{TF} = 0.1 L/min. The dashed line is an evaluation of equation 1-17, which is used to determine the saturation time at distance L/2 from the fracture.*

The perhaps biggest limitation of the models presented here and in Åkesson et al. (2010), with respect to calculating the saturation-time distribution is that we, because of the assumed symmetry, are not able to directly simulate the saturation process between two fractures with significantly different inflows. This is a common situation in the groundwater models and as such needs to be handled.

Comparing the saturation times for the same values of L/2 for fractures with different inflows it can clearly be seen that the models with $q_{TF} = 10^{-3}$ L/min (Figure 12) are saturated much faster than the models with $q_{TF} = 10^{-5}$ L/min (Figure 13).

Two examples of this are shown in Figure 14. In the left-hand graph, the ratio of saturation times for models with fracture inflow between $q_{TF} = 10^{-5}$ L/min (blue line) - 10^{-6} L/min (red line) and $q_{TF} = 10^{-3}$ L/min is shown. As can be seen, the difference in saturation time between the different fractures is greatest for small values of L/2, whereas it decreases significantly at larger values.

In the right-hand graph, the saturation time of models with $q_{TF} = 10^{-5}$ L/min (blue lines) - 10^{-6} L/min (red lines) are shown, where t_S have been normalised to the saturation time from the model with $q_{TF} = 10^{-3}$ L/min and L/2 = 170 m (dashed lines) and L/2=260 m (solid lines). The critical point here is that for fractures with $q_{TF} \leq 10^{-6}$ L/min the inflow is so low that if a fracture with $q_{TF} \leq 10^{-3}$ L/min is present anywhere in the tunnel, the latter will set the saturation time close to the low-flowing fractures, even if these are situated only a few meters apart. For fractures with $q_{TF} = 10^{-5}$ L/min the situation is somewhat more complicated, as these, if relatively closely spaced, can dominate the saturation process if the high-flowing fracture is far away.

However, we can conclude that for pairs of fractures where one has an inflow of $q_{TF} \geq 10^{-3}$ L/min and the other fracture's inflow is considerably lower, the saturation process is

PDF rendering: DokumentID 1415879, Version 1.0, Status Godkänt, Sekretessklass Öppen

completely dominated by the high flowing fracture. Thus, without simulating the situation, the best approximation is to ignore the low-flowing fracture and calculate the saturation time due to the presence of the high-flowing fracture only. This is done by taking L/2 as the distance between the fracture and the tunnel entrance or end (depending on which side of the fracture the deposition holes is situated) and taking the distance between the deposition hole and the fracture, d_{min}, into account when reading off the saturation time from the models of the tunnel-backfill saturation (Figure 12).
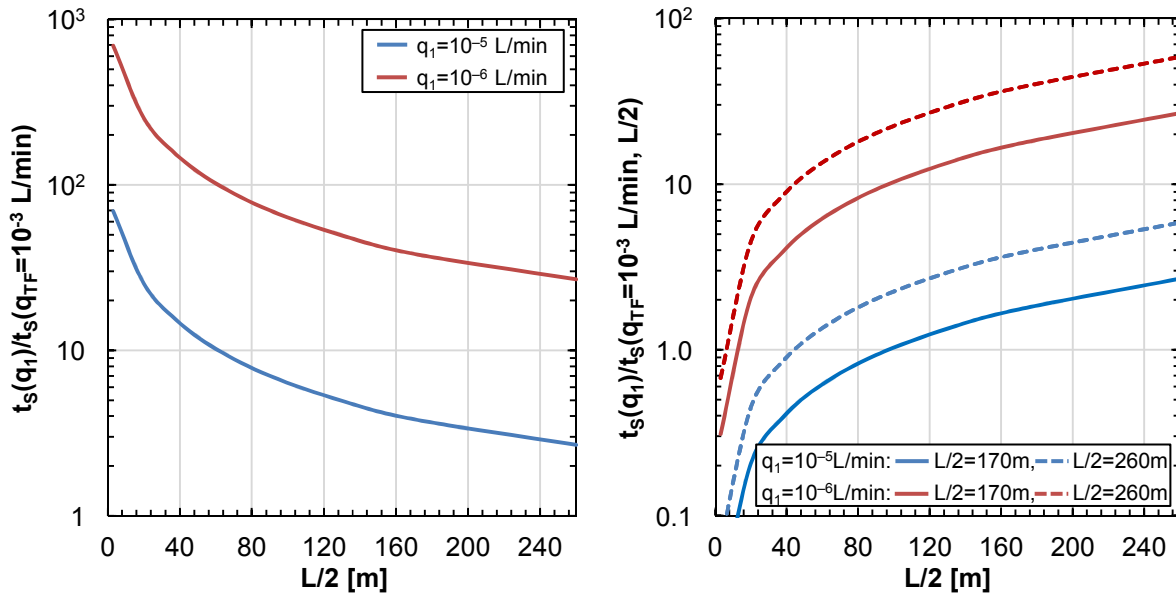

Figure 14. *The left-hand graph shows the ratio of saturation times as function of L/2 for different fracture flows (blue lines: $q_F = 10^{-5}$ L/min, red lines: $q_F = 10^{-6}$ L/min). The right-hand graph shows the saturation time for a fracture with inflow q_F, normalized to the saturation time measured for a fracture with $q_{TF} = 10^{-3}$ L/min and L/2=170 m (solid lines) and L/2=260 m (dashed lines).*

In the situation where no high-flowing fractures are present, and hence the saturation time above a deposition hole situated in between two low-flowing fractures needs to be calculated, the approach used below is to take the average inflow of the two fractures and use this in equation 1-17.

1.5   Distribution of saturation timescale

Using the model results presented above we are able to construct the expected distribution of saturation times. As a baseline we first construct the distribution assuming that no matrix flow is present. It is constructed using the following algorithm:

1) For each fracture realisation (i.e. the four different equi-probabilistic groundwater realisations r0, r2, r3 and r5 in Joyce et al 2013) all deposition holes are looped over

2) Each deposition hole is checked for intersecting fractures,

    i.   If there are intersecting fractures with an inflow higher than *0.1* L/min, the deposition hole is discarded

    ii.   if there are fractures with an inflow below *0.1* L/min, the saturation time t_{S_DHF} is taken from the results of the corresponding Code_Bright model

23

3) Then, the saturation time in the pellets column of the tunnel backfill just above the deposition hole, $t_{S\_TF}(x_{DH})$ is analysed. This is done by looping over all tunnel fractures individually and calculating $t_{S\_TF}(x_{DH})$ in two ways:

    i.   Under the assumption that the fracture in question is the only one intersecting the tunnel and thus *L/2* is the distance between the fracture and the tunnel entrance/end.

    ii.   By pairing up the fracture in question with all other fractures in the tunnel separately. Here it is vital to take into account the difference in inflow between the fractures. Given two fractures with inflow q_{TF1} and q_{TF2} we use the following approach

        a)   If both q_{TF1} and q_{TF2} are greater than *10^{-4}* L/min the saturation time is taken from the results presented in Figure 12.

        b)   If both q_{TF1} and q_{TF2} are less than *10^{-5}* L/min the saturation time is calculated using equation 1-17 and by setting $q_{TF} = (q_{TF1} + q_{TF2})/2$. The tunnel is then assumed to reach full saturation simultaneously between the two fractures.

        c)   If one fracture has an inflow greater than *10^{-4}* L/min while the other doesn't, the ratio q_{TF1}/q_{TF2} is evaluated. If *0.1* < q_{TF1}/q_{TF2} < *10*, the saturation time is again calculated by taking the average inflow between the two fractures, now using the results presented in Figure 12. However, if q_{TF1}/q_{TF2} > *10* or q_{TF1}/q_{TF2} < *0.1* the fracture pair is discarded.

The actual tunnel-backfill-saturation time at the position of the deposition hole is then taken to be the minimum value found.

4) The saturation time of the deposition hole is then taken as $t_S = \min(t_{S\_DHF},\ t_{S\_TF})$

5) If no fractures intersect the tunnel or the deposition hole, the saturation time is set equal to infinity.

The resulting saturation time is calculated for all deposition holes in all four groundwater model realisations of the Forsmark repository, and the cumulative distribution is then calculated. The result is the grey solid line in Figure 15. As can be seen the distribution has a tail towards very long saturation times, these deposition holes are situated in tunnels with very few and low flowing fractures. A small fraction (less than one per cent) of the deposition holes has an infinitely long saturation time; these are the deposition holes situated in tunnels with zero intersecting fractures.

It is, however, unrealistic to exclude matrix flow when calculating the distribution of saturation times. Measurements of the hydraulic conductivity on borehole cores from Forsmark suggests that unfractured rock samples have hydraulic conductivities between $K_M = 5 \cdot 10^{-12} - 4 \cdot 10^{-14}$ m/s under the conditions which prevail at repository depth. The saturation time of a deposition hole in the absence of fractures (i.e. through matrix flow only) has been calculated for $K_m = 10^{-11}$, 10^{-12}, 10^{-13} and 10^{-14} m/s using Code_bright models (see section 1.4.1). These results are included in Figure 15 as the coloured intervals, which are bounded by the lower (dashed lines) and upper (solid lines) limits on the saturation time as calculated from the installation and homogenised models, respectively.

For a given value of K_m, the cumulative distribution, $f(t_S)$, has the shape of the "Only fractures" distribution (grey solid line) for $t < t_S(K_M)$, while for $t \geq t_S(K_M)$ it equals one.

While this treatment is somewhat inaccurate since, if it is significant, the matrix flow will contribute to the fracture wetting and thereby change the shape of $f(t_S)$ for $t<t_S$, the error introduced should be relatively small.
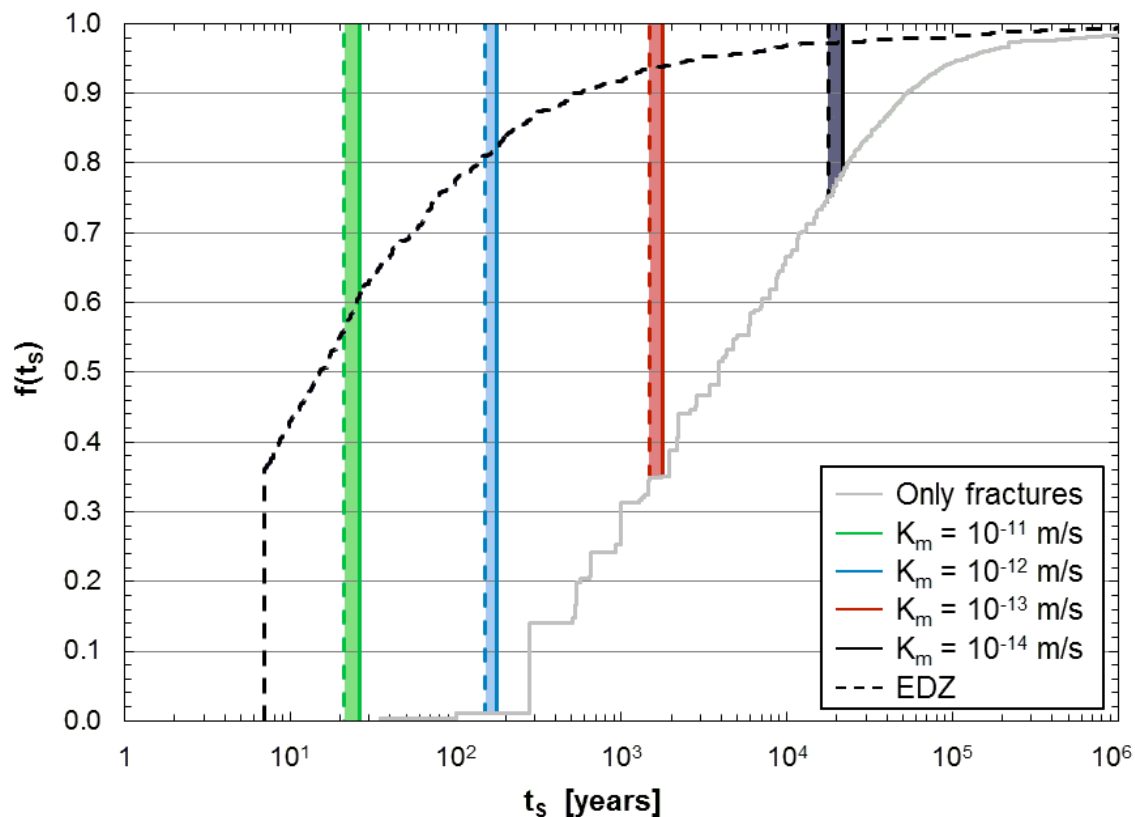

Figure 15. *The solid grey line identifies the cumulative distribution of saturation times, $f(t_S)$, in the Forsmark repository calculated assuming no matrix flow. The colored lines identify the time interval within which all deposition holes will reach full saturation if the matrix hydraulic conductivity has the value $K_m=10^{-exp}$, where exp = {11, 12, 13, 14). The dashed black line identifies the distribution of saturation times if no flow resistance was present in the tunnels (see text).*

Finally, given the rather long saturation times of a large fraction of deposition holes, it can be useful to estimate how quickly the saturation process would go if the water entering the tunnels via fractures had direct access to all parts of the tunnel instantaneously. An extremely transmissive and fully connected (along the tunnel axis) Excavation Damaged Zone (EDZ) could in theory lead to this situation. However, in Forsmark this will not be the case, as the design and construction of the repository will not allow for a highly connected EDZ to be present. More specifically the current design criteria specify that the "Excavation-induced damage should be limited and not result in a connected effective transmissivity, along a significant part (i.e. at least 20–30 m) of the disposal tunnel and averaged across the tunnel floor, higher than 10^{-8} m^2/s" (SKB 2010b). As an upper bound on how fast all deposition holes in theory could be saturated it is, however, still an interesting exercise.

If water entering through tunnel fractures is redistributed along the entire tunnel instantaneously, the saturation time of all deposition holes is to a first approximation given by the available pore volume in the deposition holes divided by the total tunnel inflow. However, this is only valid in tunnels with high inflows. If the total inflow is low, the water has time to redistribute within the bentonite, thereby leading to moisture equilibrium. The result is that

the saturation time is given by the total available pore volume in the tunnel (i.e. tunnel-backfill pore volume + deposition-hole pore volume). Then the saturation time can be calculated as:

$$t_S = \frac{V_{p,tunnel}}{q_{tunnel}} \ . \tag{1-18}$$

Here $V_{p,tunnel}$ is the total available pore volume in the tunnel and q_{tunnel} is the total inflow (through all fractures intersecting the tunnel in question) into the tunnel.

The available pore volume in the tunnel is taken to be the average volume of all tunnels (including deposition holes) and it is equal to $1.247 \cdot 10^6$ L (see Appendix). Calculating the saturation time using equation 1-18, with the data on fracture inflows as given in the groundwater models of Joyce et al. (2013) as input, result in a saturation time less than 6.9 years for approximately 35% of all deposition holes. This time is shorter than the saturation time of a deposition hole with free access to water (see Åkesson et al. 2010) and thus not valid. In these cases, the saturation time is therefore set equal to 6.9 years. The resulting distribution is shown as the black dashed line in Figure 15. It can be considered as an upper limit on how fast the deposition holes in the repository could become fully saturated in the absence of matrix flow. As can be seen in Figure 15, even for this extremely unrealistic case a significant fraction of deposition holes still takes a very long time to saturate.

1.6 Conclusions

The distribution of saturation times expected in the Forsmark repository has been analysed using a combination of 1) fracture data from groundwater models of the site and 2) Code_Bright models of the saturation process of both the deposition-hole buffer and the tunnel backfill. The resulting distribution is shown in Figure 15.

As can be seen in Figure 15 the flow properties of the so-called matrix flow are crucial when determining the distribution of saturation times. Measurements of the hydraulic conductivity of the matrix (Vilks 2007) suggest that it lies between $K_M = 5 \cdot 10^{-12} - 4 \cdot 10^{-14}$ m/s. In this range of values the effect can be summarised as:

- **High matrix conductivity ($K_m \geq 10^{-11}$ m/s):** only a tiny fraction of the deposition holes are saturated through direct fracture flow and none through water entering the deposition hole via the tunnel backfill. All deposition holes will have reached full saturation within approximately 27 years or less.

- **Intermediate matrix conductivity ($10^{-12} > K_m \geq 10^{-13}$ m/s):** between 10% and 30% of the deposition holes are saturated trough fracture flow or via water entering via the tunnel backfill. The remaining deposition holes are saturated primarily via matrix flow, all deposition holes are saturated between approximately 177 and 1760 years.

- **Low matrix conductivity ($10^{-13} < K_m \geq 10^{-14}$ m/s):** A significant fraction (30-60%) of all deposition holes are saturated via fracture flow or by water entering via the tunnel backfill. All deposition holes will have reached full saturation within approximately 22 000 years.

- **Extremely low matrix conductivity ($K_m < 10^{-14}$ m/s):** If the matrix conductivity would be extremely low almost all deposition holes will be saturated through fracture flow. Deposition holes situated in tunnels where there are no fractures will reach full saturation at a very late time, possibly after 10^6 years.

2 **Task 1.5**: Hydraulic connection between deposition holes

As part of the evaluation of SKB's license application, SSM has requested a clarification of the impact that hydraulically connected deposition holes may have on, for example, the saturation time. By hydraulic connection we here refer to the situation where two or more deposition holes are intersected by the same fracture. To analyse this question we must first answer two questions: 1) for which types of fractures is a hydraulic connection between two or more deposition holes important and 2) how common are such deposition holes in the Forsmark repository.

2.1 Relevant fracture flows

The main effect of the hydraulic connection is here assumed to be that the buffer in deposition holes upstreams in the fracture effectively dries out the fracture, significantly decreasing the fracture flow downstream. To approximately quantify when this effect may become important we must look at two aspects:

1) *The minimum required fracture flow:* In order for the hydraulic connection to be important it must be that the fracture intersecting the deposition holes have a high enough flow to be important for the saturation of the deposition hole.

2) *The maximum fracture flow that can be absorbed by a single deposition hole:* If the fracture flow is considerably higher than the flow which the bentonite can take up per unit time, the potential decrease in fracture flow due to water uptake in other deposition holes will not change the hydration evolution in the deposition hole considered.

We analyse these two limits on the fracture flow in further detail below.

2.1.1 The minimum required fracture flow

As a lower limit on the fracture flow which is interesting in this context, we can compare the saturation time due to fracture flow with the saturation time due to matrix flow. The magnitude of the matrix flow is set by the hydraulic conductivity of the matrix. The actual value of the matrix hydraulic conductivity in the Forsmark repository is, however, uncertain; a topic which was discussed in more detail in section 1.2 above. As a reference we here assume that, on the scale used in the Code_Bright models of a single deposition hole as presented in section 1.4.1, it is not lower than $K_m = 10^{-13}$ m/s.

The saturation time for $K_m = 10^{-13}$ m/s was calculated in Task 3 of Åkesson et al. (2010). The saturation time is, however, not given as a single value, but rather as a minimum and maximum time, where the uncertainty arises from the swelling of the bentonite, which is not included in the models. The saturation time for $K_m = 10^{-13}$ m/s is calculated to be between 1476 and 1760 years.

In section 1.4.1, the saturation time due to a single fracture flow is calculated. In these models, the matrix conductivity was set equal to $K_m = 10^{-14}$ m/s. Such a low value means that the matrix flow is extremely small, without the presence of a fracture it results in a saturation time between 17 742 and 21 873 years. Hence, when including a fracture in models with $K_m = 10^{-14}$ m/s the deposition hole is primarily hydrated through the fracture. The results of these models are:

Table 9. Time to 99% saturation in the deposition-hole buffer (see also section 1.4.1).

K_m [m/s]	$q_{F,0}$[1] [L/min]	t_S [years]
10^{-13}	[2]	1 476 – 1 760
10^{-14}	[2]	17 742 – 21 873
10^{-14}	10^{-1}	636.2 – 1 585.9
10^{-14}	10^{-3}	650.6 – 1 596.0
10^{-14}	10^{-5}	1 940.8 – 2 625.9

[1] The fracture flow as measured during atmospheric conditions in the deposition hole
[2] No fracture was included in these models

The results show that in deposition holes with fracture inflows less than 10^{-3} L/min (under atmospheric conditions), the saturation time is similar to that of a deposition hole which is not intersected by a fracture, but where $K_m = 10^{-13}$ m/s. Thus, in these holes the effect of any connections with other deposition holes does not significantly change the saturation evolution.

2.1.2 The maximum fracture flow

In the case of high fracture flows, the bentonite will very quickly reach full saturation just in front of the fracture. After that the inflow from the fracture cannot proceed faster than the rate at which water can be transported inside the bentonite to unsaturated parts of the buffer. This effectively puts a limit on the maximum inflow that a fracture can provide during the saturation process of the buffer. This effect is clearly seen in the model results presented in Table 9. The saturation time in the presence of a fracture with inflow (under atmospheric conditions) of 0.1 L/min is very similar to the saturation time in the presence of a fracture with inflow equal to 0.001 L/min. This can be further seen if we plot the volumetric liquid flux through the fracture from all three fracture models included in Table 9; this is shown in Figure 16. The liquid flux is almost identical in the two models with $q_{F,0} = 0.1$ and 10^{-3} L/min, whereas it is considerably lower in the model with $q_{F,0} = 10^{-5}$ L/min. This suggests that the inflow is limited by the bentonite in the first two cases, but not in the latter.

Furthermore, it can be noted that the inflow into the bentonite is significantly lower than the open fracture inflow in the models with $q_{F,0} \geq 10^{-3}$ L/min, hence such fractures should not dry out even if connected to multiple deposition holes.

2.1.3 Range of relevant open fracture inflows

We may thus conclude that the case where a fracture intersects multiple deposition holes can only have a significant effect on the saturation process if the fracture flow, as measured during open conditions, is approximately between 10^{-3} and 10^{-4} L/min, assuming that $K_m \geq 10^{-13}$ m/s in the Forsmark repository, as is indicated by measurements of the hydraulic conductivity of bore hole samples taken at the site (Vilks 2007).
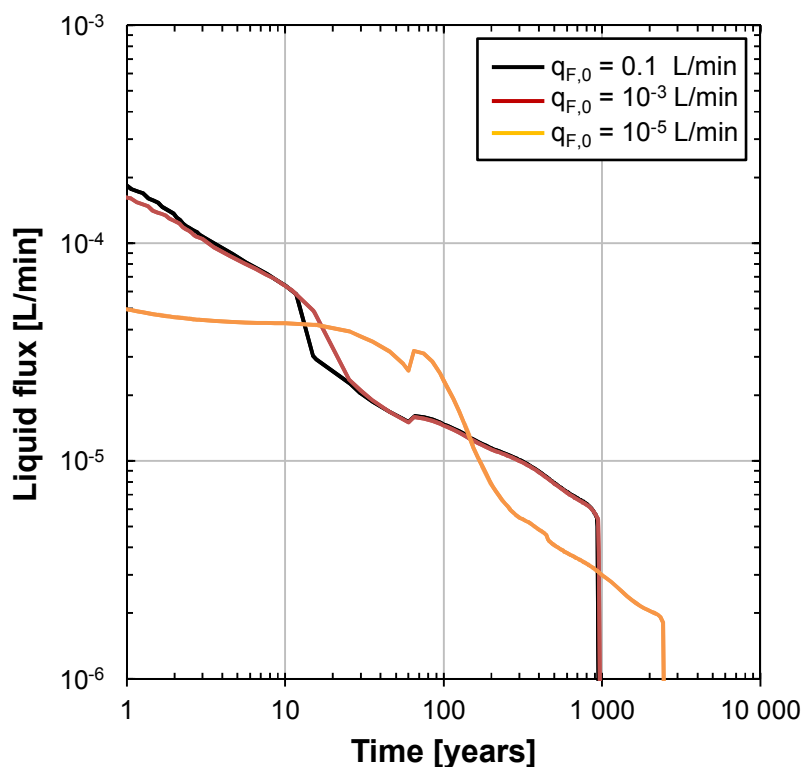
Figure 16. The flow through the fracture as function of time after installation of the buffer in the Code_Bright models discussed in section 1.4.1.

2.2 Prevalence of hydraulically connected deposition holes

To understand how common it will be that several deposition holes are intersected by a given fracture, we can use groundwater models of the Forsmark repository. In these, a fracture network has been generated given the data obtained from the surface-based site investigations at Forsmark. Here the fracture realisations r0, r2, r3 and r5 (which are equi-probabilistic realisations of the same DFN) from Joyce et al. (2013) have been used. More specifically we use the inflows and statistics on fractures intersecting deposition holes from these four realisations.

A first estimate of the prevalence of hydraulically connected deposition holes is given by the fraction of deposition holes that are intersected by one or more fractures. Taking all the data available from the groundwater models, neglecting EDZ fractures, and excluding deposition holes that share a fracture with four or more other deposition holes in the same deposition tunnel (as motivated by the Extended Full Perimeter Intersection Criterion) we find that about 10% of all deposition holes are intersected by fractures.

However, as we are only really concerned with fractures where $10^{-4} < q_F < 10^{-3}$ L/min, this fraction falls to 2.6%. Half (1.3%) of these deposition holes are intersected by a fracture which intersects at least one or several deposition holes.

2.3 Effect of hydraulic connections

The fraction of affected deposition holes (1.3%) is thus small enough that even if the effect on their saturation process were significant, the distribution of saturation times would hardly be affected.

Looking at the effect on the saturation time for an individual deposition hole we can again consider the numbers in Table 9. A deposition hole intersected by a single fracture with a flow of $q_F=10^{-3}$ L/min is saturated about twice as fast as compared to the case with no fracture but with a rock matrix conductivity of $K_m=10^{-13}$ m/s. Hence, for a given deposition hole intersected by a fracture which also intersects other deposition holes, the maximum effect, which occurs if a relatively high flowing fracture ($q_F=10^{-3}$ L/min) is entirely dried out by the buffer in other deposition holes and hence all the water enters via matrix flow, is at most a doubling of the saturation time.

The effect of hydraulic connections between deposition holes is thus, in the most extreme case, that the deposition holes in question are saturated via matrix or through tunnel backfill flow rather than through fracture flow. Since, as is discussed in Chapter 1, the majority of the deposition holes in the Forsmark repository will be saturated via matrix flow or by water entering via the tunnel backfill, deposition holes with hydraulic connections, where the saturation process is slowed down significantly, will behave as if they belong to one of these categories instead.

References

Hökmark H, Lönnqvist M, Fälth B, 2010. THM-issues in repository rock. Thermal, mechanical, thermo-mechanical and hydro-mechanical evolution of the rock at the Forsmark and Laxemar sites. Updated 2011-10, SKB TR-10-23, Svensk Kärnbränslehantering AB

Joyce S, Simpson T, Hartley L, Applegate D, Hoek J, Jackson P, Swan D,; Marsic N, Follin S, 2010. Groundwater flow modelling of periods with temperature climate conditions - Forsmark. Updated 2013-08, SKB R-09-20, Svensk Kärnbränslehantering AB.

Joyce S, Swan D, Hartley L, 2013. Calculation of open repository inflows for Forsmark. SKB R-13-21, Svensk Kärnbränslehantering AB.

SKB, 2010a. Design, production and initial state of the backfill and plug in deposition tunnels. SKB TR-10-16, Svensk Kärnbränslehantering AB.

SKB, 2010b. Design, construction and initial state of the underground openings. SKB TR-10-18, Svensk Kärnbränslehantering AB.

Svensson U, Follin S, 2010. Groundwater flow modelling of the excavation and operational phases - Forsmark. Updated 2013-08. SKB R-09-19, Svensk Kärnbränslehantering AB.

Vilks P, 2007. Forsmark site investigation – Rock matrix permeability measurements on core samples from borehole KFM01D. SKB P-07-162, Svensk Kärnbränslehantering AB.

Åkesson M, Kristensson O, Börgesson L, Dueck A, Hernelind J, 2010. THM modeling of buffer, backfill and other system components – Critical processes and scenarios. SKB TR-10-11, Svensk Kärnbränslehantering AB.

Appendix

Calculation of the average available pore volume in the deposition tunnel (MathCad excerpt):

Bentonite solid density: $\rho_s := 2.78 \cdot \dfrac{kg}{m^3}$

Liquid density: $\rho_l := 1.00 \cdot \dfrac{kg}{m^3}$

Void ratio - porosity relationship: $n(e) := \dfrac{e}{1+e}$

Saturation - Water content relationship: $S_l(w,e) := \dfrac{w \cdot \rho_s}{\rho_l \cdot e}$

Available pore volume at installation - Deposition hole

DH - Buffer ring-shaped blocks - Available pore volume:

Cross-section area : $A_R := \pi\left[(0.815 \cdot m)^2 - (0.525 \cdot m)^2\right] = 1.221 \cdot m^2$

Height: $h_R := 4.75 \cdot m$

Void ratio: $e_R := 0.571$

Water content: $w_R := 0.17$

Available pore volume: $V_{p\_R} := A_R \cdot h_R \cdot n(e_R) \cdot (1 - S_l(w_R, e_R)) = 363.216 \cdot L$

DH - Buffer cylinder-shaped blocks - Available pore volume:

Cross-section area : $A_C := \pi (0.815 \cdot m)^2 = 2.087 \cdot m^2$

Height: $h_C := 3.4 \cdot m$

Void ratio: $e_C := 0.626$

Water content: $w_C := 0.17$

Available pore volume: $V_{p\_C} := A_C \cdot h_C \cdot n(e_C) \cdot (1 - S_l(w_C, e_C)) = 669.343 \cdot L$

DH - Buffer pellets - Available pore volume:

Cross-section area : $A_P := \pi\left[(0.875 \cdot m)^2 - (0.815 \cdot m)^2\right] = 0.319 \cdot m^2$

Height: $h_P := 8 \cdot m$

Void ratio: $e_P := 1.78$

Water content: $w_P := 0.13$

Available pore volume: $V_{p\_P} := A_P \cdot h_P \cdot n(e_P) \cdot (1 - S_l(w_P, e_P)) = 1.3 \times 10^3 \cdot L$

Total DH available pore volume: $V_{p\_DH} := V_{p\_R} + V_{p\_C} + V_{p\_P} = 2.333 \times 10^3 \, L$

33

Available pore volume - Tunnel

Average tunnel length: $\quad L_T := 252 \cdot m$

Average number of deposition holes per tunnel: $\quad n_{DH} := \dfrac{6916}{207} = 33.411$

Backfill blocks (including inner slot)

Cross-section area $\quad A_{TB} := 16.8 \cdot m \cdot 1.02 \cdot m = 17.136 \, m^2$

Void ratio: $\quad e_{TB} := \dfrac{2780}{\dfrac{1700}{1.02}} - 1 = 0.668$

Water content: $\quad w_{TB} := 0.17$

Available pore volume: $\quad V_{p\_TB} := L_T \cdot A_{TB} \cdot n(e_{TB}) \cdot (1 - S_l(w_{TB}, e_{TB})) = 5.059 \times 10^5 \cdot L$

Backfill pellets

Cross-section area $\quad A_{TP} := 22.7 \cdot m^2 - 17.1 \cdot m^2 = 5.6 \, m^2$

Void ratio: $\quad e_{TP} := \dfrac{2780}{1000} - 1 = 1.78$

Water content: $\quad w_{TP} := 0.17$

Available pore volume: $\quad V_{p\_TP} := L_T \cdot A_{TP} \cdot n(e_{TP}) \cdot (1 - S_l(w_{TP}, e_{TP})) = 6.637 \times 10^5 \cdot L$

Total tunnel backfill available pore volume

$$V_{p\_T} := V_{p\_TB} + V_{p\_TP} = 1.17 \times 10^6 \, L$$

Total tunnel available pore volume (incl. deposition holes):

$$V_p := V_{p\_T} + n_{DH} \cdot V_{p\_DH} = 1.247 \times 10^6 \, L$$